

MICROMECHANICS OF REINFORCEMENT OF POLYMERS FROM 2D MATERIALS BEYOND GRAPHENE

D. G. Papageorgiou^{1*}, Ming Dong², Yi Hu¹, David Dunstan², Robert J. Young³

¹ School of Engineering and Materials Science, Queen Mary University of London, London, UK,

² School of Physical and Chemical Sciences, Queen Mary University of London, London E1 4NS, UK

³ National Graphene Institute, Henry Royce Institute and Department of Materials, School of Natural Sciences, The University of Manchester, Oxford Road, Manchester M13 9PL, U.K.

Keywords: *Micromechanics, Nanocomposites, 2D materials*

ABSTRACT

Understanding the stress transfer mechanisms from a polymer matrix to two-dimensional (2D) reinforcements is essential for the preparation of high performance nanocomposites. In the first part of this work, the interfacial stress transfer from a flexible polymer substrate to monolayer and few-layer molybdenum disulfide (MoS₂) under tension has been investigated. Layer-dependent and strain-dependent photoluminescence (PL) spectroscopy were used to examine the stress transfer efficiency. The interlayer stress transfer efficiency of MoS₂ was determined to be in the range of 0.76–0.86, higher than that of graphene. The transfer of strain from the polymer substrate to the flakes was derived through strain-dependent band shifts. With progressive loading, the strain distribution in monolayer MoS₂ can be described by the shear-lag, partial-debonding and total-debonding models.

1 INTRODUCTION

Ever since the isolation of graphene^[1], extensive research efforts have focused upon measuring the mechanical properties of graphene and other two-dimensional (2D) materials^[2]. Graphene is considered to be the strongest material with a Young's modulus of 1 TPa and a tensile strength of 130 GPa^[3]. The Young's modulus of hexagonal boron nitride (hBN) (0.86 TPa) is slightly lower than that of graphene, while the strength of hBN (70 GPa) does not degrade with the increase of layer number, up to nine layers^[4]. Molybdenum disulphide (MoS₂) is another widely-researched 2D material, mainly due to its band gap that enables application in flexible optoelectronic, spintronic and valleytronic devices^[5]. The in-plane stiffness of monolayer MoS₂ is comparable to that of steel (~270 GPa), while its fracture strength is around 23 GPa.^[6] The mechanical properties of 2D materials make them highly attractive as reinforcing agents for the fabrication of multifunctional polymer nanocomposites^[7, 8].

When 2D materials are dispersed in a polymer matrix, strain is transferred to the nanofillers via interfacial shear. As the Young's modulus of the fillers is much higher than that of the matrix, higher stresses can be sustained and mechanical reinforcement can be achieved. Therefore, understanding the stress transfer mechanism between the filler and the matrix can help towards optimization of the mechanical reinforcement of polymer nanocomposites with 2D nanofillers. Raman spectroscopy has been widely used to monitor strain in 2D materials as the strain can induce shifts in the characteristic Raman bands of 2D materials^[8-13]. Similarly, photoluminescence (PL) spectroscopy has also been used to characterize strain distribution in 2D materials with a direct band gap (such as transition metal dichalcogenides) as strain can modulate the band gap^[14-16]. Both techniques allow precise monitoring of the strain transferred from a matrix to 2D materials and facilitate the study of interfacial and interlayer stress transfer mechanisms.

The interfacial stress transfer from polymer to monolayer and few-layer MoS₂ has not been studied

quantitatively. More specifically, key parameters governing interfacial stress transfer efficiency, such as interfacial shear stress, critical transfer length and interlayer stress transfer efficiency have not been determined yet. Considering the opportunities in using monolayer and multilayer MoS₂ to reinforce polymers (see [17-19] and references therein), it is crucial to study the deformation of MoS₂ within a polymer matrix and the underlying reinforcement mechanisms. In this study, the interfacial stress transfer from a polymer matrix to monolayer and few-layer MoS₂ flakes has been investigated using in situ PL spectroscopy under strain.

2. EXPERIMENTAL SECTION

2.1 MATERIALS

A natural 2H-MoS₂ crystal with a lateral size of ~1.5 cm was purchased from HQ Graphene, Groningen, Netherlands. The tape used for the mechanical exfoliation of MoS₂ flakes was supplied by Nitto Denko Corporation, Japan. The Gel-Film used for the transfer of the flakes was procured by Gel-Pak. A commercially available poly(methyl methacrylate) (PMMA) sheet was cut into beams with length of 70 mm and width of 20 mm by laser cutting. Strain gauges with grid resistance of 120 Ω were provided by VPG Corporate.

2.2 MECHANICAL EXFOLIATION OF MoS₂

MoS₂ monolayer flakes were prepared by mechanical exfoliation of bulk MoS₂. The flakes were transferred onto a PMMA beam by an all-dry deterministic placement method. Before transfer, the PMMA beam was washed with isopropyl alcohol, was then cleaned further in an ultrasonic bath and was rinsed with DI water. The process was repeated several times to ensure the cleanliness of the substrate and after that the beam was dried using nitrogen gas. For the model nanocomposite samples, a thin layer of PMMA (4 wt% solution in methoxybenzene, 2000 rpm for 1 min, ~200 nm thickness) was spin-coated on top of the flakes.

2.5 RAMAN AND PL SPECTROSCOPY

Raman and PL spectra were collected using a micro-Raman spectrometer (Renishaw inVia) in a backscattering configuration. The laser beam was focused through a 100x objective lens with a numerical aperture (NA) of 0.9 and the laser power was kept below 0.3 mW to avoid laser heating during the experiments. The laser spot size was estimated to be about 1 μ m in diameter. For the primary characterisation of the layer number of MoS₂, PL spectroscopy was utilised using a laser excitation of 633 nm with a grating of 1200 grooves/mm and a laser excitation of 442 nm with a grating of 2400 grooves/mm. The integration time was 10 s. Raman spectroscopy was employed using a laser excitation of 442 nm with a grating of 2400 grooves/mm. The integration time was 30 s.

To deform the MoS₂ nanoflakes, the PMMA substrate with MoS₂ deposited on top of it (as illustrated in Figure 1a), was mounted on a four-point bending device. Strain was applied to the specimens in steps of about 0.05 % and the PL spectra were recorded from the middle of each flake. For line mapping measurements, the MoS₂ flakes were scanned from one end towards the centre of the specimens in steps of ~1 μ m along the loading direction.

3. RESULTS AND DISCUSSION

3.1 DEFORMATION OF MONOLAYER MOS₂

An optical image of a monolayer MoS₂ flake on the polymer substrate is shown in Figure 2b. The length of the flake along the loading direction was about 18 μ m. The PL and Raman spectra of monolayer MoS₂ are shown in Figure S1. In the monolayer MoS₂, the indirect transition gap is larger than the direct transition gap, and the smallest band gap is therefore the direct band gap at the K point [20]. As the layer

number decreases, the Raman A_{1g} mode softens due to weaker restoring forces in the vibrations, while the Raman E_{2g}^1 mode stiffens arising from either Coulomb interlayer forces or stacking-induced changes in the interlayer bonding^[21]. For monolayer MoS₂, the frequency difference between E_{2g}^1 and A_{1g} modes is the smallest ($\sim 19.2 \text{ cm}^{-1}$). These two features allow confirmation of the monolayer nature of MoS₂^[21]. The loading direction is also shown in Figure 2b (upper right) which is almost parallel to the long edge of the flake. The PL spectra of MoS₂ were collected at different strain levels. Considering the fact that the size of the flake is three orders of magnitude smaller than the length of the substrate, the flake was assumed to be strained uniaxially^[9].

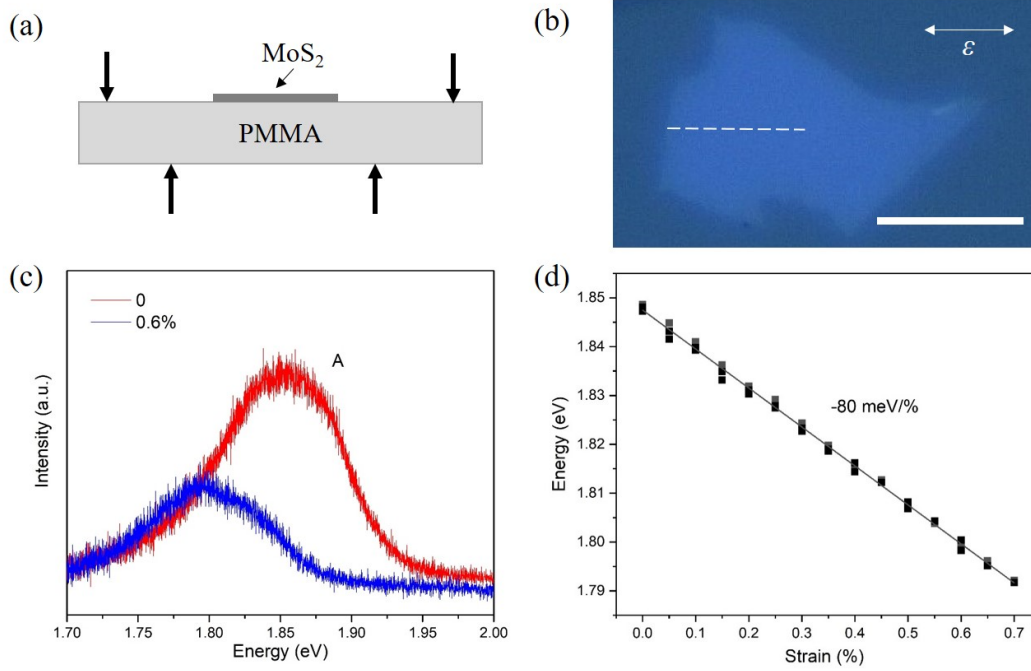


Figure 1. (a) Schematic diagram of the experimental setup, where MoS₂ flakes are supported on a PMMA substrate. (b) Optical image of a monolayer MoS₂ flake deposited on a PMMA substrate. Scale bar, 10 μm . (c) PL spectra of the monolayer flake under 0% and 0.6% strain, respectively. (d) Evolution of the A peak of the MoS₂ sample with applied strain from 0 to 0.7%.

The evolution of the PL peak measured at around the centre of the flake under strain is illustrated in Figure 1c and 1d. The principal PL peak (A peak, due to a direct band gap at the K point) was used as strain indicator because it has been shown that the A peak position provides a higher sensitivity to strain compared to Raman peak position^[22]. The A peak was fitted with a Gaussian function while the low intensity T peak was fitted with a Lorentzian function. The application of strain changes the PL spectra significantly. For the PL position, the A peak redshifted linearly with the increase of applied strain at a rate of $-80 \pm 1 \text{ meV}/\%$ (Figure 1d). The application of strain increases the Mo-Mo and Mo-S bond lengths and therefore reduces the orbital hybridization and d-bandwidth. This is reflected in the redshifted exciton resonance energies and the reduced band gap^[23]. It should be noted that the length of the exfoliated flake along the loading direction was about 18 μm , which for a monolayer flake on a PMMA substrate ($E \approx 3 \text{ GPa}$)^[22] is large enough to allow efficient stress transfer^[24]. Therefore, the strain in Figure 1d is the strain in the flake, equal to the applied strain.

It has been demonstrated that stress transfer from a polymer matrix to a flake can be monitored by mapping strain along the flake. Here, PL peak mapping was performed from the edge to the centre of the flake (dash line in Figure 1b) in steps of 1 μm , to gain an insight into the stress transfer from the polymer to monolayer MoS₂. It is necessary to convert the measured peak position to the real strain in MoS₂ flake; the band shift established in Figure 1d ($-80 \text{ meV}/\%$) was used in this calibration process. Considering the symmetry of the problem, half of the MoS₂/substrate system is illustrated here. Primarily, we need to evaluate the strain distribution in MoS₂ at low strain levels (Figure 2a). The strain

distribution can be described by the conventional shear-lag theory with the assumption of a well-bonded polymer/2D material interface. This theory predicts the strain distribution in the MoS₂ flake, ε_f , as a function of the position, x , along the loading direction,

$$\varepsilon_f(x) = \varepsilon_m \left[1 - \frac{\cosh\left(ns \frac{x}{l}\right)}{\cosh(ns/2)} \right], \quad (1)$$

where

$$n = \sqrt{\frac{2G_m}{E_f} \left(\frac{t}{T}\right)}, \quad (2)$$

is the shear-lag parameter, ε_m is the applied matrix strain, G_m is the matrix shear modulus, E_f is the Young's modulus of the flake, l is the length in the x direction, t is the thickness of the flake, T is the thickness of the representative volume and s is the aspect ratio of the flake (l/t). The solid curve in Figure 3a is the fitting of Equation 1 to the experimental data at 0.28% applied strain with $ns = 10$. The excellent agreement between the theoretical and experimental data indicate that the interface between the polymer and MoS₂ remains intact at such low strain and the strain distribution follows the expectation from shear-lag theory where the strain builds up from the edges towards the centre of the flake. The strain distribution allows the critical length l_c , which can provide indication on the quality of filler reinforcement and is small for strong interfaces, to be determined (twice the distance from the edge up to 90% of the maximum strain). At 0.28% applied strain, the critical length is estimated to be about 9 μm . This is similar with the l_c of monolayer graphene simply supported on polymer substrate (that is 10 μm for 0.5% strain), and larger than the l_c of monolayer graphene embedded between a polymer substrate and a thin polymer layer in a “model nanocomposite” configuration (3 μm for 0.4% strain). This is reasonable as the stress can be transferred to monolayer and few-layer nanoplatelets more effectively when they are embedded into a matrix. For embedded flakes, more layers adhere to the surrounding polymer which means that stress can be transferred more effectively through interfacial shear. This can minimize the possibility of slippage during loading and optimize strain transfer efficiency.

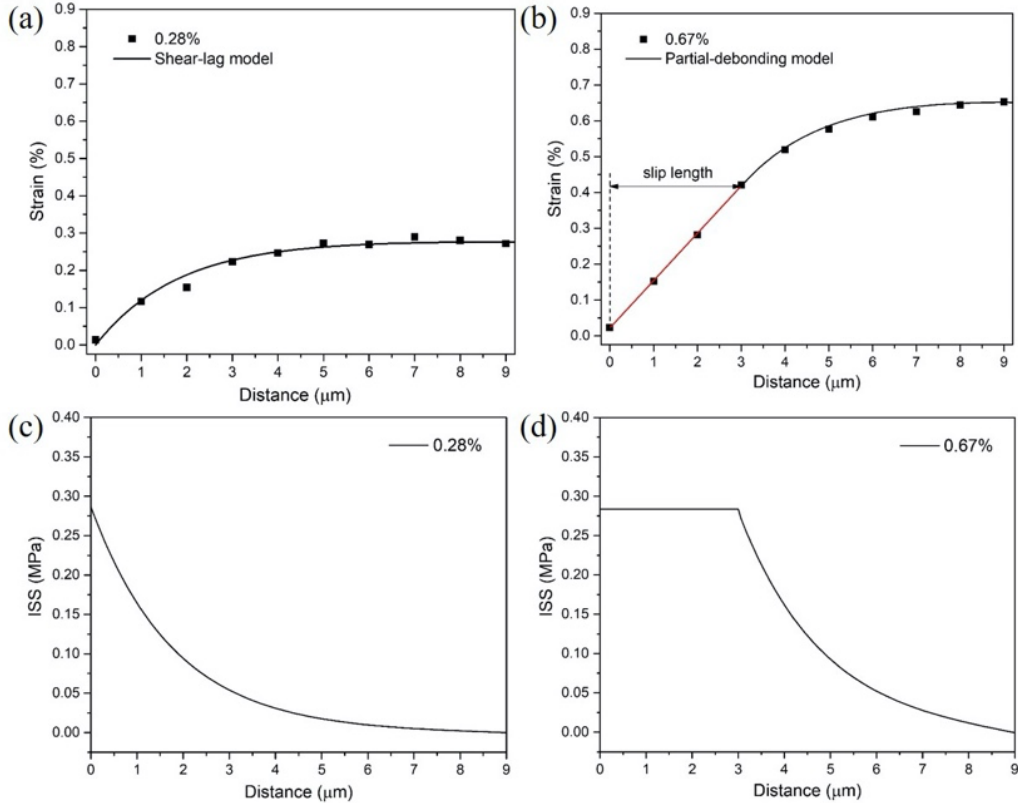


Figure 2. (a) Strain distribution in MoS₂ flake at 0.28% applied strain and the fitting result using the shear-lag model. (b) Strain distribution in MoS₂ flake at 0.67% applied strain and the fitting result using the partial-debonding model. The fitting parameter $ns = 10$ was used for both applied strains of 0.28% and 0.67%. (c) The interfacial shear stress distribution at 0.28% applied strain. (d) The interfacial shear stress and interfacial frictional stress distribution at 0.67% applied strain.

The variation of the interfacial shear stress (ISS), τ_i , can be derived by ^[24]

$$\tau_i = nE_f \varepsilon_m \frac{\sinh\left(ns \frac{x}{l}\right)}{\cosh(ns/2)} \quad (3)$$

Using the fitting parameter $ns = 10$, the length set equal to 18 μm , the thickness of monolayer MoS₂ being 0.65 nm and the Young's modulus equal to 330 GPa ^[25], the shear stress distribution curve can be derived as shown in Figure 3c. It can be seen that the ISS is maximum at the edge and decreases to zero towards the centre of the flake. The maximum ISS (interfacial shear strength, IFSS) is about 0.28 MPa. This value is similar with the one from graphene-polymer interfaces ^[24, 26, 27] and confirms the presence of van der Waals interactions between monolayer MoS₂ and the polymer matrix.

With the increase of strain, interfacial slippage will start from the ends and expand towards the centre of the flake. Similar behaviour has been observed in studies of other materials such as carbon fibres ^[28] and monolayer graphene ^[26]. In a previous study on graphene, the strain distribution after interfacial sliding was described by the nonlinear shear-lag model ^[26]. Unfortunately, by using this model, the strain in only the central part of graphene can be captured and the strain distribution near the edges (where slippage takes place) cannot be well-captured, as the shear-lag theory assumes no slippage. Herein, we show that the strain distribution in MoS₂ can be well-fitted by a partial-debonding model which has been used in the past to predict the strain distribution in carbon fibres under tension ^[28]. This model assumes that slippage occurs over a distance $ml/2$ ($0 < m < 1$) from the flake ends. In the sliding region, strain is transferred by friction and the strain distribution is almost linear as shown in Figure 2b. In the centre of the flake, the interface remains intact and strain transfer follows the classical shear-lag behaviour:

$$\varepsilon_f(x) = \varepsilon_m - \left(\varepsilon_m - \frac{4\tau_f l m}{E_f t^2} \right) \frac{\cosh\left(ns \frac{x}{l}\right)}{\cosh\left[\frac{ns(1-m)}{2}\right]} \quad (4)$$

In this case, the interfacial shear stress can be determined from the slope of the strain distribution using the force balance equation:

$$\frac{d\varepsilon}{dx} = - \frac{\tau_i}{ntE_f} \quad (5)$$

where n is the number of flake layers. By introducing the measured slope of the slippage regions into Equation 5 (0.13%/μm at 0.67% applied strain), the interfacial frictional stress is estimated to be about 0.28 MPa as shown in Figure 2d. The frictional stress at 0.46% applied strain can also be estimated at 0.26 MPa, being similar with the value at 0.67% strain. The strain distributions at 0.46% and 0.67% were also fitted using the shear-lag model and the comparison between shear-lag model and partial-debonding model is shown in Figure 3. The shear-lag model overestimates the strain in the flake when slippage takes place. In contrast, the strain distribution is well-captured by the partial-debonding model, providing a more realistic evaluation of the interfacial shear stress at higher strains. Additionally, any errors originating from the incorrect use of the shear-lag model will increase with loading as a result of the slippage length further increasing with loading.

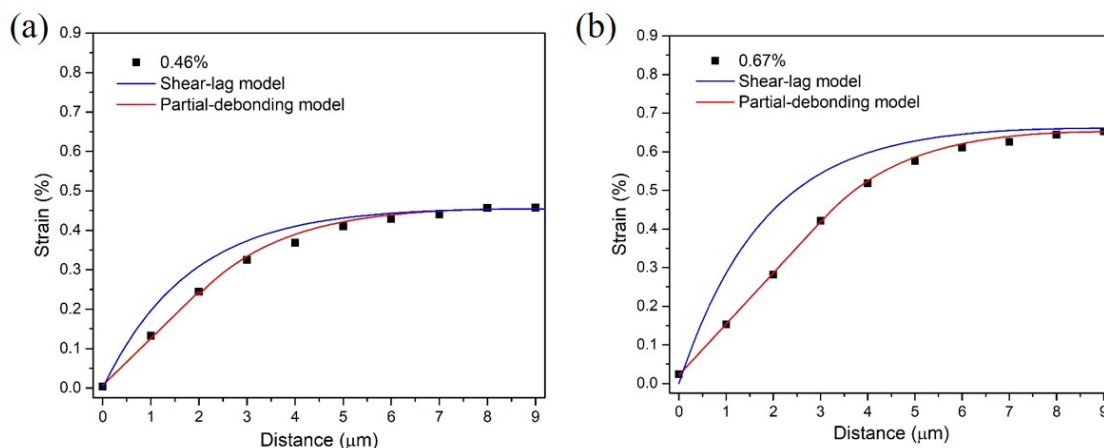


Figure 3. Strain distribution in monolayer MoS₂ at (a) 0.46% and (b) 0.67% applied strain. A comparison between the fitting curves of the shear-lag model and the partial-debonding model is presented ($ns = 10$).

CONCLUSIONS

The interfacial stress transfer from a polymer matrix to monolayer MoS₂ flakes has been studied through the application of strain *in-situ* with photoluminescence spectroscopy. The strain evolution in monolayer MoS₂ flakes follows the classic shear-lag theory at low strains and the partial-debonding and total-debonding models at higher strains. The key parameters governing the interfacial and interlayer stress transfer efficiency have been quantitatively determined. It has been demonstrated that the interfacial stress transfer efficiency between the MoS₂ layer and the matrix is similar with its graphene counterpart, while the interlayer stress transfer efficiency is higher than the one of graphene. Monolayer MoS₂ is more effective in terms of interfacial stress transfer compared to multilayer ones as the required transfer length is smaller.

REFERENCES

- [1] K. S. Novoselov, A. K. Geim, S. V. Morozov, D. Jiang, Y. Zhang, S. V. Dubonos, I. V. Grigorieva, A. A. Firsov, *Science* **2004**, *306*, 666.
- [2] C. L. Tan, X. H. Cao, X. J. Wu, Q. Y. He, J. Yang, X. Zhang, J. Z. Chen, W. Zhao, S. K. Han, G. H. Nam, M. Sindoro, H. Zhang, *Chem. Rev.* **2017**, *117*, 6225.
- [3] C. Lee, X. D. Wei, J. W. Kysar, J. Hone, *Science* **2008**, *321*, 385.
- [4] A. Falin, Q. R. Cai, E. J. G. Santos, D. Scullion, D. Qian, R. Zhang, Z. Yang, S. M. Huang, K. Watanabe, T. Taniguchi, M. R. Barnett, Y. Chen, R. S. Ruoff, L. H. Li, *Nat. Commun.* **2017**, *8*, 9.
- [5] R. Ganatra, Q. Zhang, *ACS Nano* **2014**, *8*, 4074.
- [6] S. Bertolazzi, J. Brivio, A. Kis, *ACS Nano* **2011**, *5*, 9703.
- [7] D. G. Papageorgiou, I. A. Kinloch, R. J. Young, *Prog. Mater. Sci.* **2017**, *90*, 75.
- [8] M. Dong, H. Zhang, L. Tzounis, G. Santagiuliana, E. Bilotti, D. G. Papageorgiou, *Carbon* **2021**, *185*, 57.
- [9] T. M. G. Mohiuddin, A. Lombardo, R. R. Nair, A. Bonetti, G. Savini, R. Jalil, N. Bonini, D. M. Basko, C. Galiotis, N. Marzari, K. S. Novoselov, A. K. Geim, A. C. Ferrari, *Phys. Rev. B* **2009**, *79*, 8.
- [10] C. Androulidakis, E. N. Koukaras, M. Poss, K. Papagelis, C. Galiotis, S. Tawfick, *Phys. Rev. B* **2018**, *97*, 6.
- [11] C. Rice, R. J. Young, R. Zan, U. Bangert, D. Wolverson, T. Georgiou, R. Jalil, K. S. Novoselov, *Phys. Rev. B* **2013**, *87*, 5.
- [12] F. Wang, I. A. Kinloch, D. Wolverson, R. Tenne, A. Zak, E. O'Connell, U. Bangert, R. J. Young, *2D Mater.* **2017**, *4*, 14.

- [13] D. G. Papageorgiou, Z. Li, M. Liu, I. A. Kinloch, R. J. Young, *Nanoscale* **2020**, *12*, 2228.
- [14] H. J. Conley, B. Wang, J. I. Ziegler, R. F. Haglund, S. T. Pantelides, K. I. Bolotin, *Nano Lett.* **2013**, *13*, 3626.
- [15] I. Niehues, A. Blob, T. Stiehm, R. Schmidt, V. Jadrisko, B. Radatovic, D. Capeta, M. Kralj, S. M. de Vasconcellos, R. Bratschitsch, *2D Mater.* **2018**, *5*.
- [16] F. Carrascoso, H. Li, R. Frisenda, A. Castellanos-Gomez, *Nano Res.* **2021**, *14*, 1698.
- [17] M. Ahmadi, O. Zabihi, S. Jeon, M. Yoonessi, A. Dasari, S. Ramakrishna, M. Naebe, *J. Mater. Chem. A* **2020**, *8*, 845.
- [18] X. Wang, W. Y. Xing, X. M. Feng, L. Song, Y. Hu, *Polym. Rev.* **2017**, *57*, 440.
- [19] A. S. Sethulekshmi, J. S. Jayan, S. Appukuttan, K. Joseph, *Physica E* **2021**, *132*, 20.
- [20] K. F. Mak, C. Lee, J. Hone, J. Shan, T. F. Heinz, *Phys. Rev. Lett.* **2010**, *105*, 4.
- [21] C. Lee, H. Yan, L. E. Brus, T. F. Heinz, J. Hone, S. Ryu, *ACS Nano* **2010**, *4*, 2695.
- [22] Z. Liu, M. Amani, S. Najmaei, Q. Xu, X. L. Zou, W. Zhou, T. Yu, C. Y. Qiu, A. G. Birdwell, F. J. Crowne, R. Vajtai, B. I. Yakobson, Z. H. Xia, M. Dubey, P. M. Ajayan, J. Lou, *Nat. Commun.* **2014**, *5*, 9.
- [23] K. He, C. Poole, K. F. Mak, J. Shan, *Nano Lett.* **2013**, *13*, 2931.
- [24] L. Gong, I. A. Kinloch, R. J. Young, I. Riaz, R. Jalil, K. S. Novoselov, *Adv. Mater.* **2010**, *22*, 2694.
- [25] A. Castellanos-Gomez, M. Poot, G. A. Steele, H. S. J. van der Zant, N. Agrait, G. Rubio-Bollinger, *Adv. Mater.* **2012**, *24*, 772.
- [26] T. Jiang, R. Huang, Y. Zhu, *Adv. Funct. Mater.* **2014**, *24*, 396.
- [27] C. Androulidakis, D. Surlantzis, E. N. Koukaras, A. C. Manikas, C. Galiotis, *Nanoscale Adv.* **2019**, *1*, 4972.
- [28] M. A. Montes-Moran, R. J. Young, *Carbon* **2002**, *40*, 857.